Electron beam induced current and remote electron beam induced current assessment of chemical vapor deposited diamond films

A. Cremades and J. Piqueras

Citation: J. Appl. Phys. **85**, 1438 (1999); doi: 10.1063/1.369275
View online: http://dx.doi.org/10.1063/1.369275
View Table of Contents: http://jap.aip.org/resource/1/JAPIAU/v85/i3
Published by the American Institute of Physics.

Electron beam induced current and remote electron beam induced current assessment of chemical vapor deposited diamond films

A. Cremades and J. Piqueras[a)]
Departamento de Física de Materiales, Facultad de Físicas, Universidad Complutense, Madrid 28040, Spain

(Received 27 July 1998; accepted for publication 27 October 1998)

In the present work, electron beam induced current (EBIC) has been applied to characterize several kinds of chemical vapor deposition diamond films. Regions of enhanced carrier recombination are detected in plan-view observations of thin films as well as in cross sections of thick films. Remote EBIC (REBIC) has been applied to obtain information about charged defects present in the samples. The dependence of EBIC and REBIC contrast on the contact configuration used, and on the observation conditions has been analyzed. Cathodoluminescence images of the same samples have been recorded for comparison. © *1999 American Institute of Physics.* [S0021-8979(99)07303-X]

I. INTRODUCTION

The possibility of application of diamond films in optoelectronic devices has attracted much attention in the past years.[1–4] The use of characterization techniques able to provide spatially resolved information about electronic recombinations and local conduction processes is of interest in studies of charge carrier properties related to optoelectronic applications. One of these techniques is the cathodoluminescence in the scanning electron microscope (CL-SEM), which has been often applied to investigate radiative recombination processes in diamond.[5–8] However, electron beam induced current (EBIC), which is another scanning electron micrograph (SEM) based technique, has been mainly applied to semiconductors, seldom to dielectric films, and only occasionally to diamond.[9–11] The information provided by EBIC relates to recombination processes and to the effect of charged defects on local properties.

In the present work the capability of EBIC to characterize diamond films has been investigated in detail. In particular, EBIC has been applied to thin samples with different textures or grain orientations and cross-sectional observations of thick samples have been carried out. In order to perform a more complete study of the capability of beam induced current techniques, remote EBIC (REBIC) has been used in the films characterization. Application of REBIC to characterize diamond films has not been, to our knowledge, previously reported. CL-SEM has been used as a complementary technique.

II. EXPERIMENT

The samples used were polycrystalline chemical vapor deposition (CVD) diamond films. All thin layers (8 μm) were grown on (100) boron-doped silicon with the same nucleation procedure, but different textured growth steps in order to obtain both (100) oriented films and films without significant texture, as reported elsewhere.[9,12] These samples will be hereinafter referred to as (100) oriented and nonoriented films, respectively. The samples were sputtered with a 10 nm Ti layer followed by 15 nm Au, after annealing in air at 500 °C for 15 min. This treatment increases the surface resistance by about four orders of magnitude.[13] Other samples used were thick films from Norton Co., with a thickness of about 300 μm. These samples had a gold metallized surface.

The samples were observed in the secondary electron, EBIC and CL modes in a Hitachi S-2500 SEM at accelerating voltages ranging from 10 to 30 kV, beam currents of 10^{-9}–10^{-6} A, and at temperatures between 100 and 300 K. For EBIC and REBIC measurements, contacts were provided by silver paint with gold wires, following the contact configurations shown in Figs. 1 and 2. EBIC signal was detected with a Matelec ISM5 induced current monitor. During the experiments no qualitative contrast changes were observed in the temperature range between 100 and 300 K, so that the images presented here were recorded at room temperature. Panchromatic CL images were recorded at 100 K using a Hamamatsu R928 photomultiplier attached to a window of the SEM chamber. A lens inside the chamber focused the light onto the window.

III. RESULTS

A. EBIC measurements

EBIC images obtained for thin diamond films, recorded using the contact configuration (a) of Fig. 1, are shown in Figs. 3(a) and 3(b). The images correspond to regions of metallized diamond in the two kind of samples: (100) oriented films [Fig. 3(a)], and nonoriented films [Fig. 3(b)]. The Ti/Au contact deposited on the diamond surface acts as a potential barrier which separates carriers of both signs generated in the sample by the incident electrons. Bright contrast on the images appears associated to an efficient carrier collection, and hence high beam induced current, while dark contrast is due to enhanced carrier recombination which reduces the EBIC signal. It can be observed in Fig. 3(a) that (100) faces of epitaxial oriented grown films show dark contrast while intergranular regions appear bright. In the images

a)Electronic mail: piqueras@eucmax.sim.ucm.es

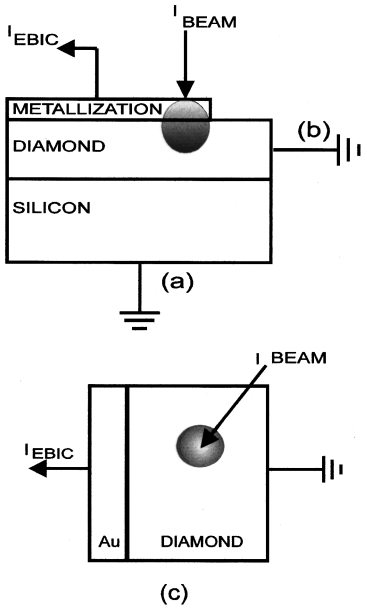

FIG. 1. Contact configurations used for: (a) and (b) plan-view EBIC measurements on thin films, and (c) cross-section measurements on thick films. The figure is not scaled.

of the nonoriented films, it is difficult to assign a particular crystal face to dark or bright features due to their complex morphology. Nevertheless, it can be observed that the intergranular regions of these films present bright contrast. Figures 3(c) and 3(d) show, for comparison, the panchromatic CL images of the same samples. Bright regions in the CL image of (100) epitaxial films [Fig. 3(c)] are identified with (100) crystal faces. For nonoriented samples [Fig. 3(d)], the

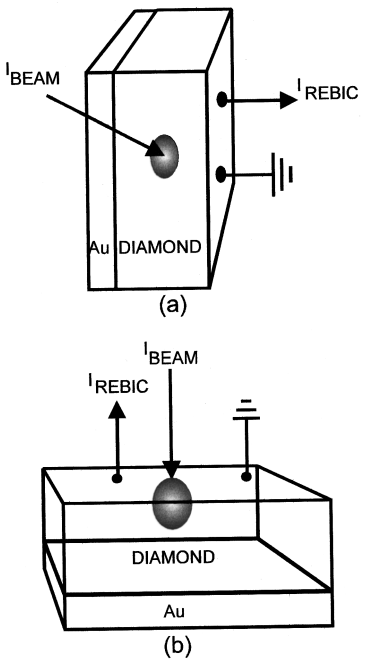

FIG. 2. Contact configurations used for REBIC measurements of (a) cross section and (b) upper surface of thick samples.

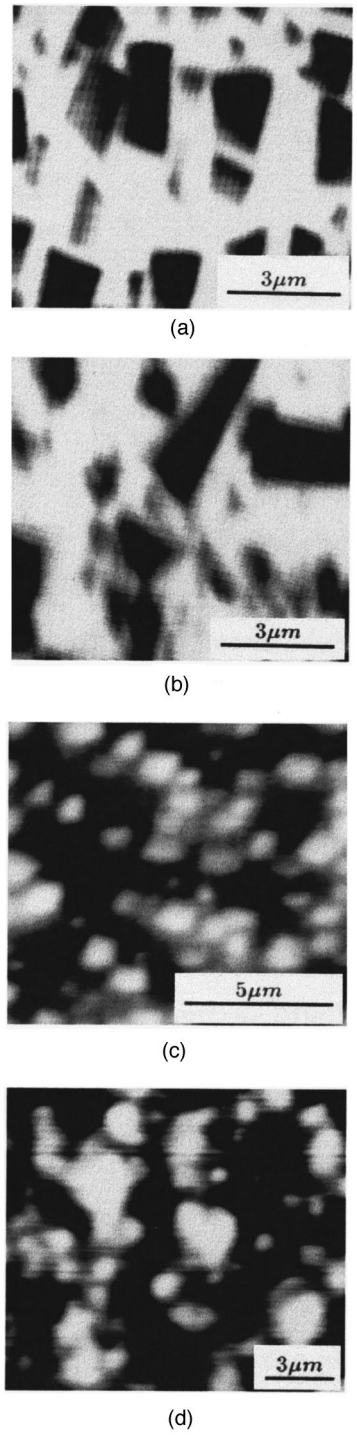

FIG. 3. EBIC images of the upper surface of (a) a (100) epitaxial grown film and (b) a homogeneous nonoriented film and CL images (c) and (d) of the same films, respectively.

CL intensity does not follow any pattern due to the large range of grain sizes and the different faces exposed to the beam.

The 300-μm-thick Norton film was used for cross-sectional observations. In these measurements the contact configuration (c) shown in Fig. 1 was used. The metallized surface was the potential barrier for the EBIC measurements and the opposite surface of the sample was contacted by

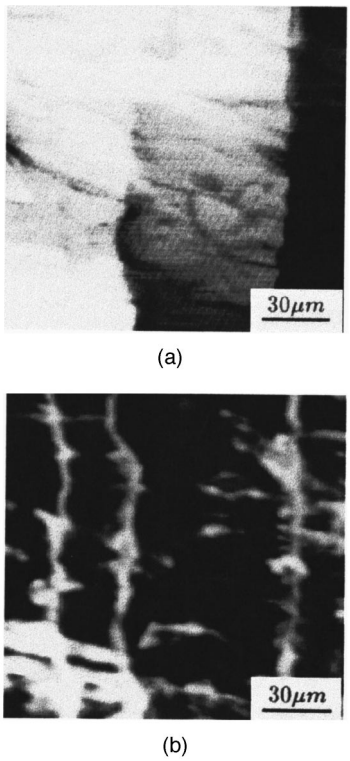

FIG. 4. (a) EBIC and (b) CL images of the same cross section.

means of gold wire and silver paint. Figure 4 shows an EBIC image of the cross section and the CL image of the same region. The images present a pattern which consists of same bright lines for the CL image and dark lines on a bright background for the EBIC image. The lines, whose main direction is parallel to the upper sample surface will be hereinafter called *A* lines, and lines mainly directed in the perpendicular direction will be referred to as *B* lines. Details of the cathodoluminescence characterization of this film have been previously reported.[5]

The dependence of the EBIC current detected near the metallized surface on the beam accelerating potential E, the beam diameter (d_0), and the angular aperture (α_p) of the electron beam was measured. These parameters are related to the beam excitation current[14] and therefore the EBIC current is obtained as a function of the beam current I_b. A barrier efficiency of about 1.96×10^{-5} was estimated from the expression

$$I_{\mathrm{EBIC}}=\eta_{\mathrm{cc}}GI_b,$$

where η_{cc} is the collection efficiency of the barrier and G is the pair generation coefficient.

B. REBIC measurements

The contact configurations used for the measurements in thin films are those marked as (a) and (b) in Fig. 1. Contrary to the case of EBIC, to record a REBIC image, the beam probe scans nonmetallized diamond zones far apart from the metallization barrier. The barrier is not able to separate carriers generated by the beam in points of the sample at a distance of several millimeters.

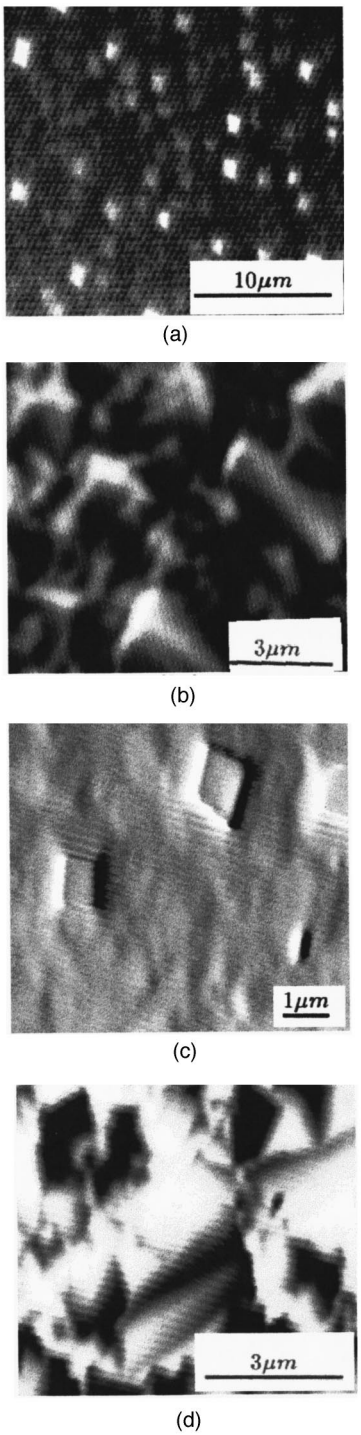

FIG. 5. REBIC images with the metallization-silicon contact configuration of (a) (100) epitaxial film and (b) homogeneous film; and REBIC images with metallization-diamond contacts of (c) (100) epitaxial film and (d) homogeneous film.

Figure 5 shows the images [5(a) and 5(b)] of both thin samples recorded with the (a) contact configuration (metallization silicon), and those recorded for the metallization-diamond contacts [contact configuration (b)] [5(c) and 5(d)]. In Fig. 5(a) it is observed that (100) faces present bright contrast. As in the EBIC images it is difficult to identify bright areas in the image of the nonoriented films due to its complex morphology [Fig. 5(b)]. The (100) epitaxial films

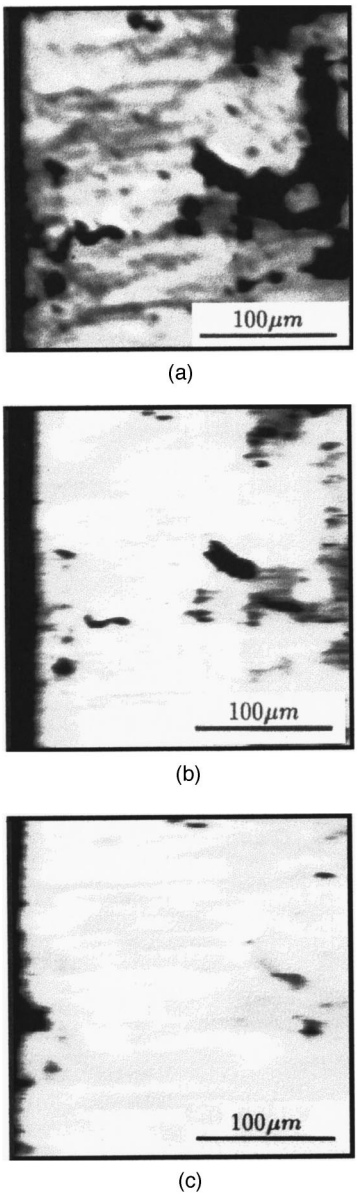

FIG. 6. REBIC images of the cross section for different excitation conditions: (a) 4.9×10^{-9} A, (b) 9.1×10^{-8} A, and (c) 5.6×10^{-7} A.

present different contrast when the (b) contact configuration is used [Fig. 5(c)]. This contrast is known as white–black contrast or peak and trough, and has been observed in REBIC measurements of different materials.[15,16] The change in contact configuration also modifies the contrast associated to the nonoriented sample, as observed in Fig. 5(d). In this case grains and intergranular bright regions are observed.

For the REBIC images of the thick film we have used the contact configurations shown in Fig. 2, which correspond to observations of the cross section and of the upper surface of the sample, respectively. Both contacts are located in the nonmetallized surface and consist of gold wires and silver paint. In Fig. 6, contrast due to the different excitation conditions used in the measurements of the cross section are observed. The REBIC contrast due to the charged defects detected in these images depends on the value of the beam

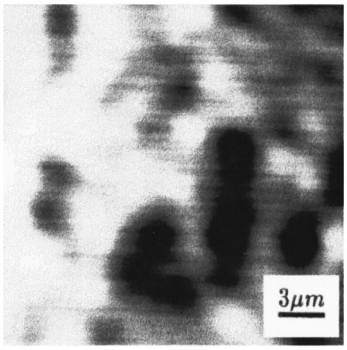

FIG. 7. REBIC image of the upper surface of the thick sample.

excitation current. For low values of the beam current [Fig. 6(a)], two kinds of defects related, respectively, to lines *A* and *B* can be observed. When the beam current increases over 10^{-6} A, *A* lines related defects are not detectable, while the contrast associated to *B* lines disappears for excitation densities over 10^{-7} A.

The plan-view images of the thick sample (Fig. 7) show a gradual signal intensity increase from the right to the left side due to the resistance of diamond between the contacts. A cell-like structure is also observed in Fig. 7.

IV. DISCUSSION

A. EBIC

The EBIC signal is formed by the carriers of different sign separated by the electrical field in the barrier and collected by the contacts. The electron–hole pairs that contribute to the EBIC signal are a fraction of the total number generated by the incident beam because some pairs recombine through defect centers before they are able to reach the contacts. In regions with high concentration of recombination centers, the EBIC signal is low (gray or black points in the images), and on the contrary, bright regions are an indication of an efficient carrier separation by the barrier and carrier collection.

The results obtained for the contact configuration (a) of Fig. 1, clearly indicate that (100) faces of epitaxial oriented films are regions of enhanced recombination, while in the intergranular zones the EBIC signal is higher [Fig. 3(a)]. In the homogeneous films, some crystals faces, in addition to intergranular regions, show a high level of EBIC signal [Fig. 3(b)]. EBIC contrast of epitaxial films is qualitatively similar with both contact configurations (a) and (b). This indicates that the symmetry of the potential barrier [metallization diamond (100)] is high and the signal does not depend on the direction of carrier motion to the contacts. This situation changes for the nonoriented films, in which all grains appear with dark contrast for the second configuration of contacts. This is an indication of lower symmetry of the barrier formed by the metallization on the nonoriented diamond.

The comparison between CL and EBIC images of the epitaxial samples [Figs. 3(a) and 3(c)] shows the existence of enhanced radiative recombination in the (100) faces, which causes a low EBIC signal and a high CL intensity in these faces. The recombination centers have been identified, by

means of CL spectroscopy,[9] as defects related to silicon incorporation in the films, nitrogen–vacancy complexes, and point defects associated to dislocations which cause blue emission. The present results show that EBIC applied to diamond films is able to reveal regions of enhanced recombination, especially in crystals with a regular morphology such as the (100) oriented grains. The comparison between CL and EBIC results of nonoriented samples[9] enables the identification of radiative centers which cause dark contrast in EBIC images as centers related to dislocations and nitrogen–vacancy complexes. Due to the complex crystal morphology, the enhanced recombination cannot be related to (100) faces [Figs. 3(b) and 3(d)].

The EBIC measurements on thick films provide an example of cross-section characterization. The image of Fig. 4 shows that the regions of preferent recombination appear as dark lines whose main direction is parallel to the upper sample surface (*A* lines), as well as lines mainly directed in the perpendicular direction, or *B* lines. This structure corresponds to the columnar grain structure often described in CVD diamond samples[17,18] and already detected by CL measurements.[5]

As described above, the cross-sectional EBIC measurements enable one to calculate the metallization-diamond barrier efficiency. The value obtained of 1.96×10^{-5} is very low compared with the efficiency of $p-n$ silicon junctions, calculated also from EBIC measurements.[19] In diamond, due to its high electrical resistance, the distance that carriers move under an applied electric field is very low ($\lambda<1\ \mu$m) relative to the separation between contacts ($D=300\ \mu$m). The material between the contacts acts as a parallel plane capacitor, decreasing the efficiency by a factor $1/D$, as Gunn[20] and Dearneley[21] concluded for dielectric materials. This fact explains that the EBIC current is comparable and even less than the excitation current although the estimated values for the generation factor is about 10^3 electron–hole pairs per 30 kV incident electron. The same effect has been observed in other materials like semi-insulating GaAs and ZnS.[22]

The CL study of the cross section of these samples[5] shows that *A* lines contain a high concentration of radiative centers related to nitrogen–vacancy complexes, while *B* lines are mainly related to the emission of centers aggregated at dislocations. These centers are responsible for the EBIC dark contrast in the images, but a contribution of the nonradiative centers to the EBIC contrast cannot be ruled out.

B. REBIC

The REBIC mode is mainly applied to dielectric films. The electrically charged defects present in the material act as local potential barriers in which carriers are separated. Due to the high resistance of the diamond film and the distance between contacts, the signal profile shows a pronounced slope, which remains constant in regions with the same local conductivity. This effect is observed as a gradation or intensity gradient from one side to the other in the REBIC images. The EBIC signal arising from charged defects is superimposed on this background.

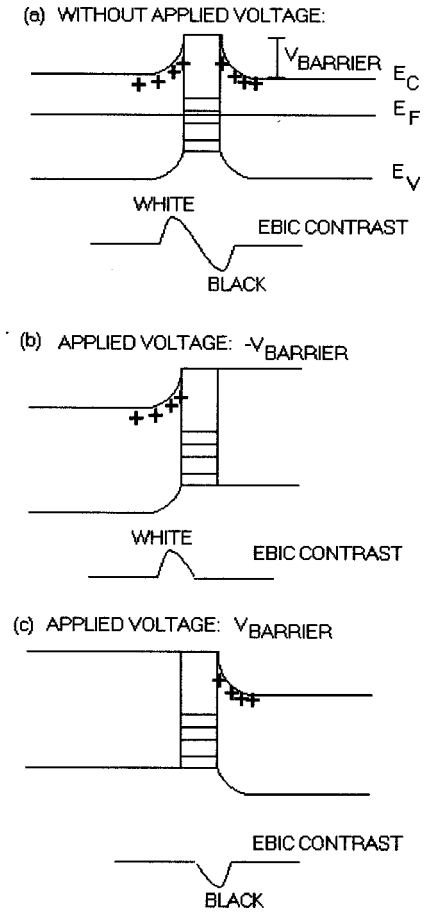

FIG. 8. Generation of the white–black contrast: (a) with no applied voltage, (b) with $-V_{\text{barrier}}$ bias voltage, and (c) with V_{barrier} forward voltage.

A characteristic REBIC contrast of charged defects,[15,16] known as black–white contrast, appears at defects in which the local electric field has opposite directions at each side of the barrier as Fig. 8(a) shows.

This contrast can be modeled by two Schottky barriers back to back[23] and it depends on the contact configuration and on the orientation of the beam scanning direction relative to the defect barrier. Therefore by changing these experimental conditions, the black–white contrast can be converted into only black or only white contrast. The same effect is obtained by the application of a bias or reverse voltage as observed in the schema of Fig. 8.

Images of the epitaxial oriented films [Fig. 5(a)] show black–white contrast as well as the dependence of the contrast white or black–white on the contact configuration. The REBIC contrast associated to diamond grains is an indication of the presence of charged defects in the grains. On the contrary, the nonoriented films show electrical activity of grains and of intergranular regions. An inversion of the REBIC contrast of the nonoriented films by changing the contact configuration, is observed in Figs. 5(b) and 5(d).

The REBIC images of diamond thick layers (Fig. 6) show two different charged defects with dark to white contrast depending on the excitation density used during measurements. Defects located between *A* lines described in Sec. I of the discussion, and defects located in *B* lines will be

referred to as *A* and *B* defects, respectively. The potential barrier associated to *A* defects disappears when the beam current is over 10^{-6} A, while the barrier related to *B* defects is readily compensated by beam injection over 10^{-7} A. The effect of increasing excitation density is similar to polarizing the defect potential barrier as in Fig. 8.

When the beam injection causes a compensation of the charge state of the defect, the associated barrier disappears, which causes the suppression of the defect contrast.

Due to the configuration of contacts used in the REBIC of the cross section (both contacts are located at the surface of the sample), no gradation of the image intensity is observed. However, this effect is clearly observed in the REBIC images recorded on the surface. This is the case of Fig. 7, in which the REBIC profile associated with a line of this image presents a pronounced slope. Superimposed on it appears the EBIC signal related to charged defects that typically corresponds to dislocations, precipitates, and grain boundaries.[15,16,24]

V. CONCLUSIONS

EBIC measurements on diamond films reveal regions of enhanced recombination. These regions correspond mainly to (100) faces in (100) epitaxial oriented thin films. EBIC cross-sectional observations of thick films reveal a pattern of dark lines which can be identified as grain boundaries in the columnar structure of the sample. EBIC images show an approximate opposite contrast to the CL images of the same regions. The value of the efficiency of the metallization-diamond barrier has been estimated.

In the REBIC mode a contrast has been observed, similar to that previously reported for other dielectric materials. REBIC appears to be a useful technique to the study of local electrical properties of diamond films. In both modes, EBIC and REBIC, the influence of the contacts configuration and the excitation conditions on the observed contrast has been determined.

ACKNOWLEDGMENTS

This work has been supported by DGICYT (Project PB96-0639). Thanks are due to Professor Dr. M. Schreck and Dr. R. Hessmer for growing the thin films, and Professor Dr. E. Wolfgang for providing the thick samples.

[1] I. M. Buckley-Golder and A. T. Collins, Diamond Relat. Mater. **1**, 1083 (1992).
[2] M. G. Geis and J. Angus, Sci. Am. **266**, 64 (1992).
[3] B. Buchard, A. M. Zaitser, W. R. Fahner, A. A. Malnikov, A. V. Denisenko, and V. S. Varichenko, Diamond Relat. Mater. **3**, 947 (1994).
[4] J. D. Hunn, S. P. Withrow, C. W. White, R. E. Clausing, L. Haetherly, and C. P. Christensen, Appl. Phys. Lett. **65**, 3072 (1994).
[5] A. Cremades, F. Dominguez-Adame, and J. Piqueras, J. Appl. Phys. **74**, 5726 (1993).
[6] A. Cremades and J. Piqueras, J. Appl. Phys. **78**, 3353 (1995).
[7] A. Cremades, J. Piqueras, and J. Solis, J. Appl. Phys. **79**, 8118 (1996).
[8] L. H. Robins, L. P. Cook, E. N. Farabaugh, and A. Feldman, Phys. Rev. B **39**, 13367 (1989).
[9] A. Cremades, J. Piqueras, and M. Schreck, Diamond Relat. Mater. **6**, 95 (1997).
[10] R. Heiderhoff, P. Koschinski, M. Maywald, L. J. Balk, and P. K. Bachmann, Diamond Relat. Mater. **4**, 645 (1995).
[11] K. Okano, H. Kiyota, T. Iwasaki, T. Kurosu, M. Iida, and T. Nakamura, Appl. Phys. Lett. **58**, 840 (1991).
[12] M. Schreck, R. Hessmer, S. Geier, B. Rauschenbach, and B. Strizker, Diamond Relat. Mater. **3**, 510 (1994).
[13] R. Hessmer, M. Schreck, S. Geier, and B. Strizker, Diamond Relat. Mater. **3**, 951 (1994).
[14] L. Reimer, *Scanning Electron Microscopy*, Springer Series in Optical Science (Springer, Berlin, 1985), Vol. 45, Chap. 2.
[15] G. Panin and E. Yakimov, Semicond. Sci. Technol. **7**, 150 (1992).
[16] D. B. Holt, B. Raza, and A. Wojcik, Mater. Sci. Eng., B **42**, 14 (1996).
[17] H. A. Hoff, C. J. Craigie, E. Dantsker, and C. S. Pande, Appl. Phys. Lett. **59**, (1991).
[18] K. V. Ravi, C. A. Koch, H. S. Hu, and A. Joski, J. Mater. Res. **5**, 2356 (1990).
[19] D. B. Holt, in *Quantitative Scanning Electron Microscopy*, edited by D. B. Holt, M. D. Muir, P. R. Grant, and I. M. Boswara (Academic, London, 1974), Chap. 8.
[20] J. B. Gunn, Solid-State Electron. **7**, 739 (1964).
[21] G. Dearnaley and D. C. Northrop, *Semiconductor Counters for Nuclear Radiations* Spon. London 75 (1966).
[22] D. B. Holt, E. Napchan, A. Wojcik, M. Ammou, and P. Gibart, Inst. Phys. Conf. Ser. **134**, 731 (1993).
[23] E. Ziegler, W. Siegel, H. Blumtritt, and O. Breitenstein, Phys. Status Solidi A **72**, 593 (1982).
[24] G. N. Panin and E. B. Yakimov, J. Phys. (Paris), Colloq. **C6**, 181 (1991).